NASA/TM—2004-212480 ARL–TR–3014

Defect Clustering and Nanophase Structure Characterization of Multicomponent Rare Earth-Oxide-Doped Zirconia-Yttria Thermal Barrier Coatings

Dongming Zhu
U.S. Army Research Laboratory, Glenn Research Center, Cleveland, Ohio

Yuan L. Chen
QSS Group, Inc., Cleveland, Ohio

Robert A. Miller
Glenn Research Center, Cleveland, Ohio

January 2004

The NASA STI Program Office . . . in Profile

Since its founding, NASA has been dedicated to the advancement of aeronautics and space science. The NASA Scientific and Technical Information (STI) Program Office plays a key part in helping NASA maintain this important role.

The NASA STI Program Office is operated by Langley Research Center, the Lead Center for NASA's scientific and technical information. The NASA STI Program Office provides access to the NASA STI Database, the largest collection of aeronautical and space science STI in the world. The Program Office is also NASA's institutional mechanism for disseminating the results of its research and development activities. These results are published by NASA in the NASA STI Report Series, which includes the following report types:

- TECHNICAL PUBLICATION. Reports of completed research or a major significant phase of research that present the results of NASA programs and include extensive data or theoretical analysis. Includes compilations of significant scientific and technical data and information deemed to be of continuing reference value. NASA's counterpart of peer-reviewed formal professional papers but has less stringent limitations on manuscript length and extent of graphic presentations.

- TECHNICAL MEMORANDUM. Scientific and technical findings that are preliminary or of specialized interest, e.g., quick release reports, working papers, and bibliographies that contain minimal annotation. Does not contain extensive analysis.

- CONTRACTOR REPORT. Scientific and technical findings by NASA-sponsored contractors and grantees.

- CONFERENCE PUBLICATION. Collected papers from scientific and technical conferences, symposia, seminars, or other meetings sponsored or cosponsored by NASA.

- SPECIAL PUBLICATION. Scientific, technical, or historical information from NASA programs, projects, and missions, often concerned with subjects having substantial public interest.

- TECHNICAL TRANSLATION. English-language translations of foreign scientific and technical material pertinent to NASA's mission.

Specialized services that complement the STI Program Office's diverse offerings include creating custom thesauri, building customized databases, organizing and publishing research results . . . even providing videos.

For more information about the NASA STI Program Office, see the following:

- Access the NASA STI Program Home Page at ***http://www.sti.nasa.gov***

- E-mail your question via the Internet to help@sti.nasa.gov

- Fax your question to the NASA Access Help Desk at 301–621–0134

- Telephone the NASA Access Help Desk at 301–621–0390

- Write to:
  NASA Access Help Desk
  NASA Center for AeroSpace Information
  7121 Standard Drive
  Hanover, MD 21076

NASA/TM—2004-212480 ARL–TR–3014

Defect Clustering and Nanophase Structure Characterization of Multicomponent Rare Earth-Oxide-Doped Zirconia-Yttria Thermal Barrier Coatings

Dongming Zhu
U.S. Army Research Laboratory, Glenn Research Center, Cleveland, Ohio

Yuan L. Chen
QSS Group, Inc., Cleveland, Ohio

Robert A. Miller
Glenn Research Center, Cleveland, Ohio

National Aeronautics and
Space Administration

Glenn Research Center

January 2004

Acknowledgments

This work was supported by the NASA Ultra-Efficient Engine Technology (UEET) Program. The authors are grateful to George W. Leissler and Ralph Garlick at the NASA Glenn Research Center for their assistance in the preparation of plasma-sprayed thermal barrier coatings and x-ray diffraction, respectively, and to Robert W. Bruce at General Electric Aircraft Engines and Kenneth S. Murphy at Howmet Research Corporation for electron-beam-physical-vapor-deposited (EB–PVD) coating processing.

Available from

NASA Center for Aerospace Information
7121 Standard Drive
Hanover, MD 21076

National Technical Information Service
5285 Port Royal Road
Springfield, VA 22100

Available electronically at http://gltrs.grc.nasa.gov

Defect Clustering and Nanophase Structure Characterization of Multicomponent Rare Earth-Oxide-Doped Zirconia-Yttria Thermal Barrier Coatings

Dongming Zhu
U.S. Army Research Laboratory
National Aeronautics and Space Administration
Glenn Research Center
Cleveland, Ohio 44135

Yuan L. Chen
QSS Group, Inc.
Cleveland, Ohio 44135

Robert A. Miller
National Aeronautics and Space Administration
Glenn Research Center
Cleveland, Ohio 44135

Summary

Advanced thermal barrier coatings (TBCs) have been developed by incorporating multicomponent rare earth oxide dopants into zirconia-based thermal barrier coatings to promote the creation of thermodynamically stable, immobile oxide defect clusters and/or nanophases within the coating systems. In this report, the defect clusters, induced by Nd, Gd, and Yb rare earth dopants in the zirconia-yttria thermal barrier coatings, were characterized by high-resolution transmission electron microscopy (TEM). The TEM lattice imaging, selected area diffraction (SAD), and electron energy-loss spectroscopy (EELS) analyses demonstrated that extensive nanoscale rare earth dopant segregation exists in the plasma-sprayed and electron-beam-physical-vapor-deposited (EB–PVD) thermal barrier coatings. The nanoscale concentration heterogeneity and the resulting large lattice distortion promoted the formation of parallel and rotational defective lattice clusters in the coating systems. The presence of the 5- to 100-nm-sized defect clusters and nanophases is believed to be responsible for the significant reduction of thermal conductivity, improved sintering resistance, and long-term high-temperature stability of the advanced thermal barrier coating systems.

Introduction

Thermal barrier coatings (TBCs) are technologically important because of their ability to further increase engine operating temperatures and reduce cooling, thus achieving engine efficiency and emission goals. To help meet future engine design and advanced coating requirements, efforts have been made to develop significantly lower conductivity and better high-temperature stability TBCs, primarily by incorporating multicomponent rare earth oxide dopants into the current zirconia-yttria-based thermal barrier coatings (refs. 1 and 2 and Zhu, D.; and Miller, R.A.: Defect Cluster Design Considerations in Advanced Thermal Barrier Coatings. Unpublished work, NASA Glenn Research Center, Cleveland, Ohio, 1999.). The added dopants are intended to create thermodynamically stable, highly defective lattice structures with essentially immobile defect clusters and/or nanoscale ordered phases—thereby reducing thermal conductivity and improving sintering resistance of the coating systems. Multicomponent thermal

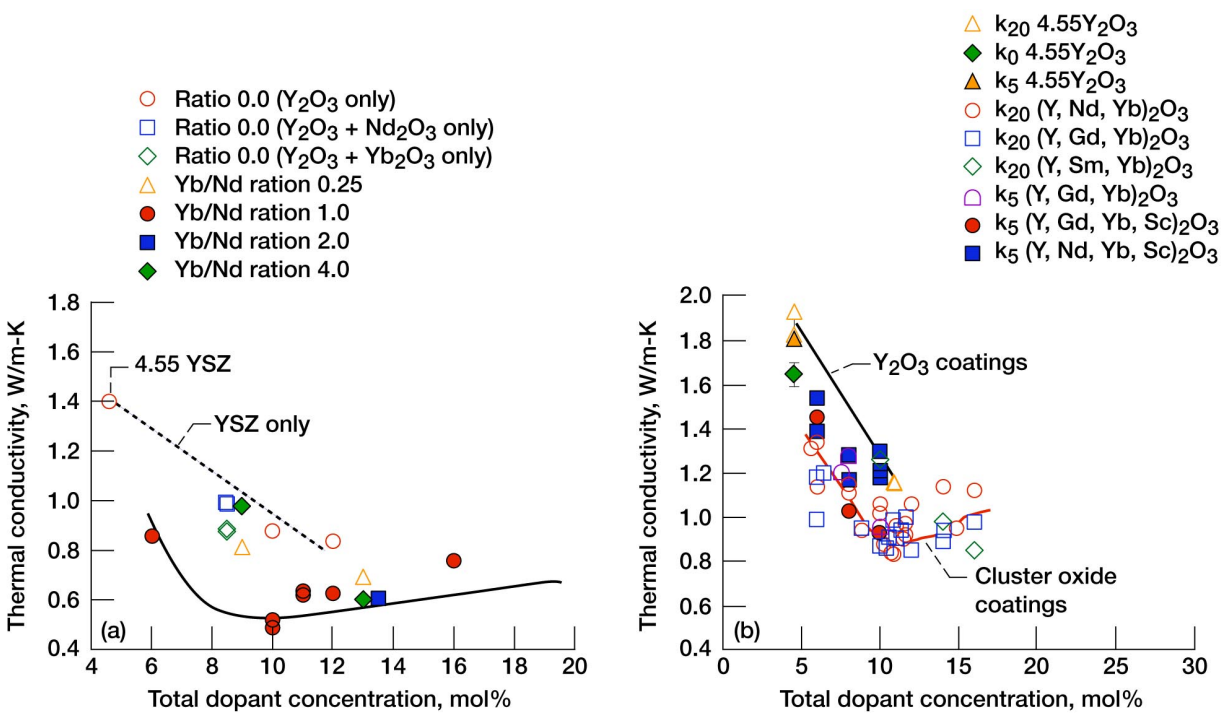

Figure 1.—Thermal conductivity as function of total dopant concentration for baseline ZrO_2-4.55 mol% Y_2O_3 (ZrO_2-8 wt% Y_2O_3) and multicomponent ZrO_2-Y_2O_3-based coatings, determined by laser heat flux technique at 1316 °C. (a) Plasma-sprayed coatings after 20 h of sintering testing at 1316 °C. (b) Initial thermal conductivity k_0 with 5-h- and 20-h-sintering thermal conductivities, k_5 and k_{20}, respectively, of EB–PVD coatings.

barrier coatings have been shown to reduce the TBC thermal conductivity by a factor of 2 or 3 compared with a baseline ZrO_2-4.55 mol% Y_2O_3 (ZrO_2-8 wt% Y_2O_3) coating at high temperature, as shown in figure 1. In addition, the sintering resistance of the coating systems has also been reduced by one order of magnitude, in terms of the steady-state conductivity rate increase shown in figure 2, presumably due to the low-mobility defect cluster effect associated with the rare earth dopant additions.

The purpose of this report is to investigate the dopant defect clustering phenomena in ZrO_2-Y_2O_3 multicomponent plasma-sprayed and electron-beam-physical-vapor-deposited (EB–PVD) thermal barrier systems using high-resolution transmission electron microscopy (TEM). Dopants studied include Nd_2O_3, Gd_2O_3, Yb_2O_3, and Sc_2O_3. In this study, the dopant segregation as well as the dopant-heterogeneity-induced defect cluster formation were investigated using high-resolution TEM lattice imaging, selected area diffraction (SAD), electron energy-loss spectroscopy (EELS) and energy-dispersive spectroscopy (EDS) analysis techniques. The defect cluster size and distribution, cluster crystallographic orientation, and defective lattice distortion are also estimated based on the TEM lattice moiré fringe analysis. The defect clustering information is of great importance in understanding the thermal conductivity, sintering behavior, and thermomechanical performance of the multicomponent TBCs. The nanostructural oxide defect information is also critical to the development of advanced high-temperature TBCs with unique thermophysical and thermomechanical properties.

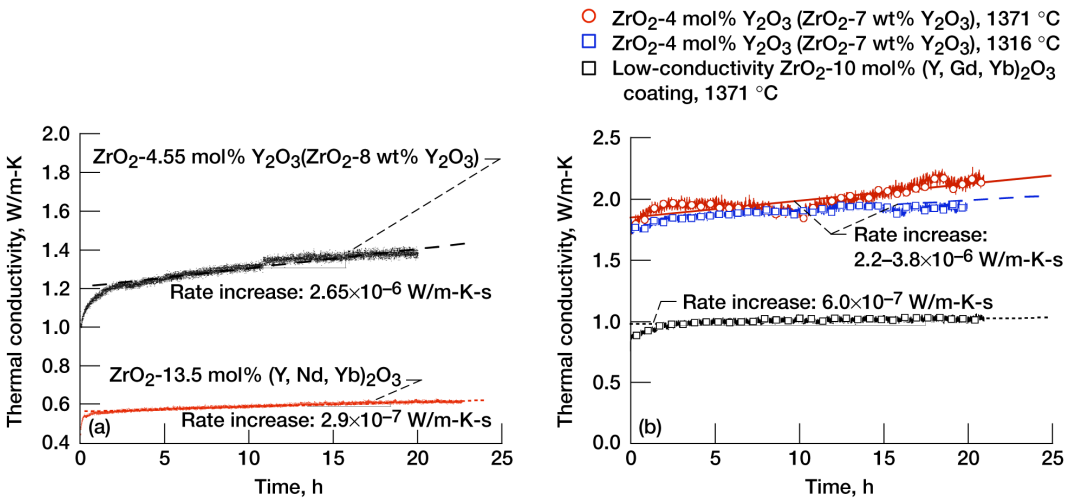

Figure 2.—Thermal conductivity of plasma-sprayed and EB–PVD coatings as function of time under steady-state heat-flux temperature testing, illustrating conductivity rate increase. (a) Plasma-sprayed low-conductivity ZrO_2-13.5 mol% $(Y, Nd, Yb)_2O_3$ and baseline ZrO_2-4.55 mol% Y_2O_3 coatings tested at 1316 °C; (b) EB–PVD low-conductivity ZrO_2-10 mol% $(Y, Gd, Yb)_2O_3$ and baseline ZrO_2-4 mol% Y_2O_3 coatings tested at 1316 and 1371 °C.

Experimental Materials and Method

Multicomponent oxide thermal barrier coatings were designed using a oxide defect-clustering approach described previously (refs. 1 and 2 and Zhu, D.; and Miller, R.A.: Defect Cluster Design Considerations in Advanced Thermal Barrier Coatings. Unpublished work, NASA Glenn Research Center, Cleveland, Ohio, 1999.). In the present study, four-component, defect-clustered oxide thermal barrier coating systems, i.e., plasma-sprayed ZrO_2-13.5 mol% $(Y, Nd, Yb)_2O_3$ and EB–PVD ZrO_2-12 to 14 mol% $(Y, Gd, Yb)_2O_3$ coatings, were selected for the TEM defect cluster investigation. Several five-component plasma-sprayed and EB–PVD coatings with Sc_2O_3 additions (which partially replace some of Yb_2O_3) were also studied under TEM. In the coating systems, the main stabilizer dopant Y_2O_3 has a larger concentration compared with the paired cluster dopants, Nd_2O_3 (or Gd_2O_3) and Yb_2O_3 (and/or Sc_2O_3). These compositions were selected only as examples for the defect cluster structural studies and thus may not represent the optimum compositions for coating performance. The advanced thermal barrier coating systems, typically consisting of a 180- to 250-μm ceramic top coat and a 75- to 120-μm NiCrAlY or PtAl intermediate bond coat, were plasma sprayed or electron beam physical vapor deposited onto the 25.4-mm-diameter and 3.2-mm-thick nickel base superalloy René N5 disk substrates. The plasma-sprayed coatings were processed using all NASA in-house fabricated, pre-alloyed powders. The ceramic powders with the designed composition were first spray dried, then plasma reacted twice and spheroidized to ensure the composition and phase homogeneity, and finally plasma sprayed into the coating form in the NASA Glenn plasma-spray coating facilities. The advanced EB–PVD coatings were deposited using prefabricated evaporation ingots that were made of the desired composition. The EB–PVD coatings were processed into test coating specimens by General Electric Aircraft Engines, Cincinnati, Ohio, and Howmet Coatings Corporation, Whitehall, Michigan. The plasma-sprayed and EB–PVD disk coating specimens were furnace annealed at 1000 °C for 24 h and then laser heat-flux treated at 1316 °C for 20 h before they were examined in the TEM. X-ray diffraction techniques were used for the coating phase identification and lattice constant estimation.

The TEM structural investigation of the defect-clustered coatings was carried out using a Philips CM200 transmission electron microscope (FEI Company, Hillsboro, OR). In order to prepare the TEM specimens, the coating specimens were first cross sectioned into thin slices. The sliced ceramic coatings were glued with a degassed epoxy mixture and sandwiched between two Si dummy wafers. The sandwiched specimens were then sliced to a size of 2.5 by 2.0 by 0.5 mm. The final TEM specimens were thinned to electron transparency using argon-ion-beam milling for a short period of time to polish both sides. Diffraction contrast and high-resolution images as well as SAD data for the coating specimens were recorded using the TEM operating at 200 keV. The elemental analysis was conducted using an EDAX energy dispersive spectrometer (EDAX, Inc., Mahwah, NJ) and an electron energy loss spectrometer attached to the TEM system.

Results and Discussion

Phase Structures and Lattice Constants of Defect Cluster Coatings

The x-ray diffraction results showed that the oxide defect cluster coatings have the predominant tetragonal phase structure when the yttria and paired rare earth dopant concentration is lower than 6 mol%. The coatings adopt the cubic phase structure when the total dopant concentration is higher than 10 mol% (ref. 3). The x-ray diffraction patterns of selected oxide coatings are shown in figure 3.

The diffraction peaks shift towards lower diffraction angle with increasing dopant concentration, indicating that the ZrO_2-based oxide lattice constant increases with the dopant concentration. The addition of the paired rare earth cluster oxide dopants, e.g., Nd with Yb or Nd with Sc, to the ZrO_2-Y_2O_3 system has further increased the oxide lattice constants. Note that this occurs when even only one of the paired cluster dopant oxide has a larger ionic size than the primary dopant yttria in the multicomponent oxide systems. Figure 4(a) shows the lattice constants of several plasma-sprayed and EB–PVD ZrO_2-Y_2O_3 and ZrO_2-Y_2O_3-Nd_2O_3-Yb_2O_3(and/or Sc_2O_3) coatings as a function of dopant concentration, determined by the x-ray diffraction techniques. It can be seen that the lattice constant of the multicomponent oxide coating systems has increased by 1 to 2 percent in the dopant concentration range of 5 to 16 mol%. Furthermore, as shown in figure 4(b), the cluster dopants have also broadened the x-ray diffraction peaks, implying larger lattice distortion for the multicomponent oxide coatings.

TEM Observation of Defect Clusters

Figure 5 shows high-resolution TEM lattice images of the cubic plasma-sprayed Zr-13.5 mol% (Y, Nd, Yb)$_2O_3$, the EB–PVD Zr-12 mol% (Y, Nd, Yb)$_2O_3$, and the plasma-sprayed ZrO_2-6 mol% (Y, Nd, Yb, Sc)$_2O_3$ thermal barrier coatings. Parallel moiré fringe regions are observed in the TEM (111) plane lattice images in near-(110) orientation, with the typical contrast region size ranging from 5 to 40 nm (50 to
400 Å). This is in contrast to the pseudobinary ZrO_2-Y_2O_3 coatings case where the moiré patterns have not been observed under a similar coating treatment condition. The parallel moiré fringe regions are formed because of the overlapping lattices having different lattice constants (thus the different lattice plane *d*-spacing values) within the multicomponent thermal barrier coatings. Because the coatings have a single-phase cubic structure, the formation of the nanometer-sized parallel moiré fringe regions within the TBC grain strongly suggests a large variation of the lattice spacing in a small-sized region due to the rare earth cluster dopant segregations and compositional heterogeneities. The TEM moiré fringe patterns demonstrate the presence of the defect clusters in the TBCs caused by the incorporation of the rare earth dopants.

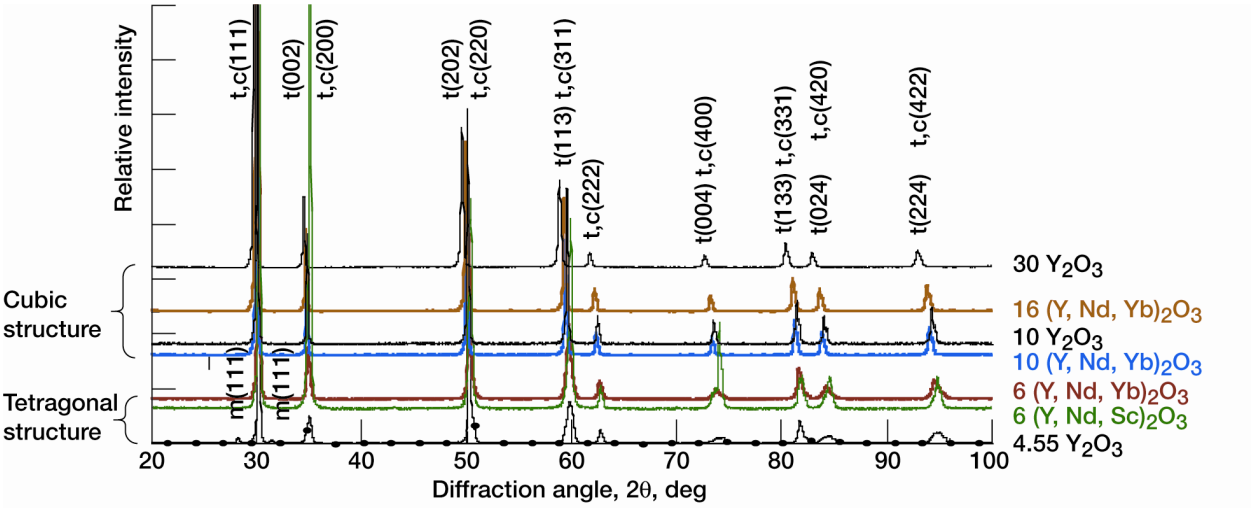

Figure 3.—X-ray diffraction patterns of selected oxide thermal barrier coatings, where tetragonal and cubic structures are represented by “t” and “c,” respectively.

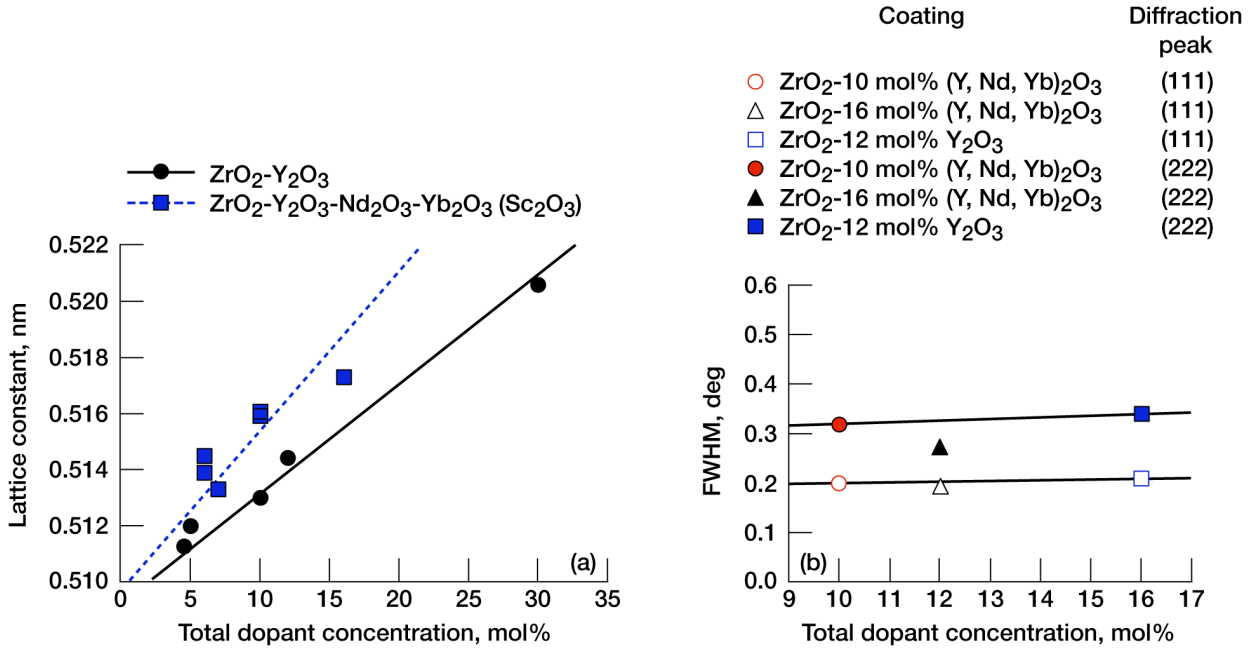

Figure 4.—Lattice constants and x-ray diffraction peak width of ZrO_2-Y_2O_3 and ZrO_2-Y_2O_3-Nd_2O_3-Yb_2O_3(Sc_2O_3) coatings as function of dopant concentration. (a) Lattice constants. (b) Full-width half-maximum (FWHM) of (111) and (222) diffraction peaks for some cubic-phased coatings.

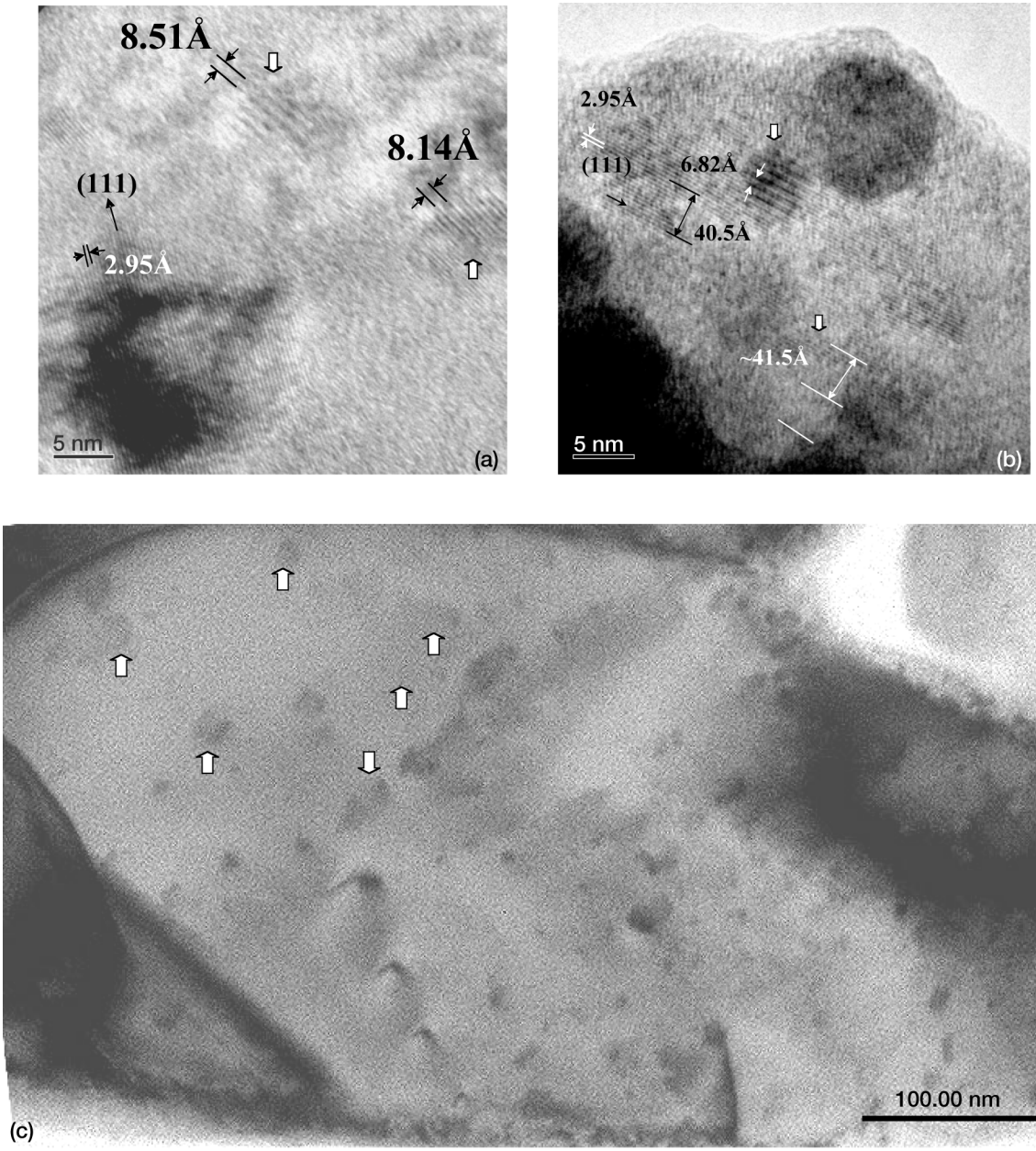

Figure 5.—High-resolution TEM lattice images showing Nd-, Yb-, and Sc-induced defect clusters (indicated by large arrows) in near-(110) orientation in Nd and Yb (and/or Sc) co-doped ZrO_2-Y_2O_3 thermal barrier coatings. (a) Plasma-sprayed ZrO_2-13.5 mol% (Y, Nd, Yb)$_2O_3$ coating. (b) EB–PVD ZrO_2-12 mol% (Y, Nd, Yb)$_2O_3$ coating. (c) Plasma-sprayed ZrO_2-6 mol% (Y, Nd, Yb, Sc)$_2O_3$ coating.

The observed parallel moiré fringe pattern spacing in the (111) lattice images is typically found to be in the range of 0.6 to 0.9 nm (6 to 9 Å). In certain regions, the parallel moiré fringes with a larger spacing of 4 to 5 nm (40 to 50 Å) are also observed. The relationship between the parallel moiré fringe pattern D_p and the two contrasting lattice spacings d_1 and d_2 can be expressed by (ref. 4)

$$D_p = \frac{d_1 d_2}{|d_1 - d_2|} \tag{1}$$

Therefore, assuming that the average lattice spacing of the (111) plane $d_1(111)$ is approximately 0.295 nm (corresponding to the lattice constant $a_1 \approx$ 0.511 nm) in the segregation-free region, the lattice spacing $d_2(111)$ and the lattice parameter a_2 in the cluster region can be estimated from the observed moiré fringes spacing D_p. It is found that the parallel moiré fringe regions with a smaller fringe spacing of 0.6 to 0.9 nm (6 to 9 Å) correspond to the overlapping lattices of (111) and (100), while the moiré patterns with a larger spacing of 4 to 5 nm (40 to 50 Å) roughly correspond to the two overlapping (111) lattice planes that have distinct *d*-spacing values because of the dopant segregation. Figure 6 shows the estimated lattice constants in the dopant-segregated cluster regions derived from the parallel moiré patterns of overlapping (111) and (100) lattice planes. The average lattice constant is about 0.53 to 0.54 nm (5.3 to 5.4 Å) in the dopant-segregated region, as compared to the assumed lattice constant 0.511 nm (5.11 Å) in the nonsegregating region. On average, the local dopant segregation caused 4- to 6-percent strains because of the lattice distortion.

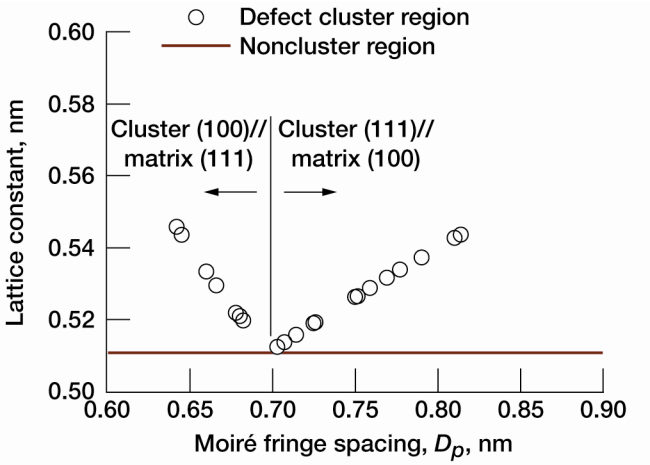

Figure 6.—Estimated lattice constants in cluster-dopant-segregated regions derived from (111) and (100) plane parallel moiré patterns in near-(110) orientation.

Mixed moiré patterns are also often observed in the multicomponent coating systems because of the overlapping lattices with combined lattice rotation and *d*-spacing variation. Figure 7 shows the mixed moiré patterns of a plasma-sprayed, Nd and Yb co-doped multicomponent thermal barrier coatings. The dopant cluster regions, observed as the moiré patterns in the TEM lattice images, typically have a size of 10 to 20 nm (100 to 200 Å), with the moiré fringe spacing ranging from 0.7 to 5 nm (7 to 50 Å). A large defect clustered region in an EB–PVD Gd and Yb co-doped ZrO_2-Y_2O_3 coating that has a size larger than 50 nm (500 Å) and a moiré fringe spacing about 0.7 nm (7 Å) is shown in figure 8.

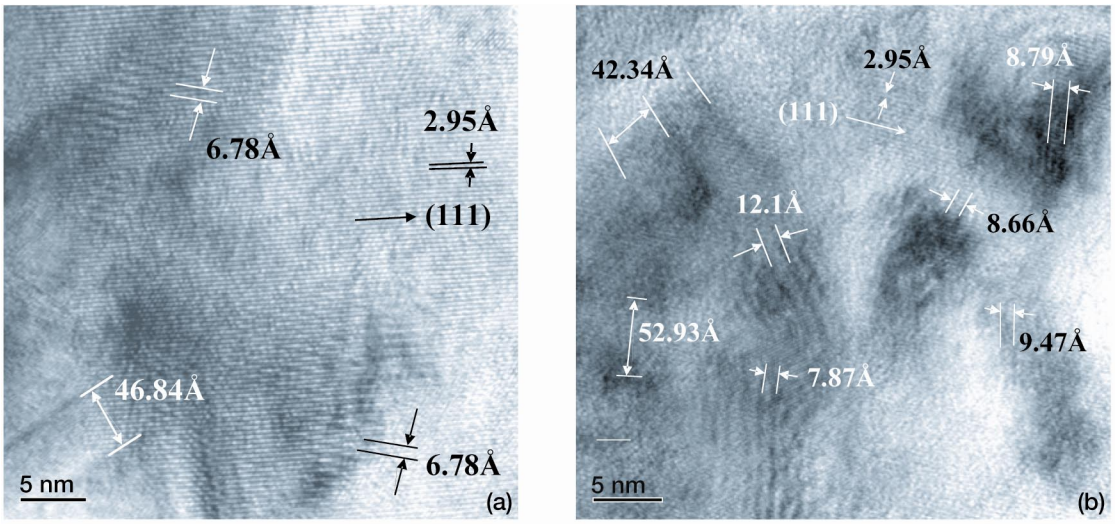

Figure 7.—High-resolution TEM (111) lattice images in near-(110) orientation showing defect clusters in plasma-sprayed ZrO_2-13.5 mol% $(Y, Nd, Yb)_2O_3$ thermal barrier coating, observed as mixed moiré patterns. Two different cluster regions are shown.

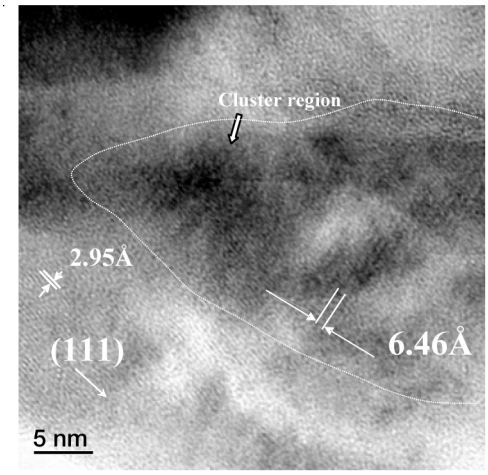

Figure 8.—High-resolution TEM (111) lattice image in near-(110) orientation showing defect clusters in EB–PVD ZrO_2-14 mol% $(Y, Gd, Yb)_2O_3$ thermal barrier coating.

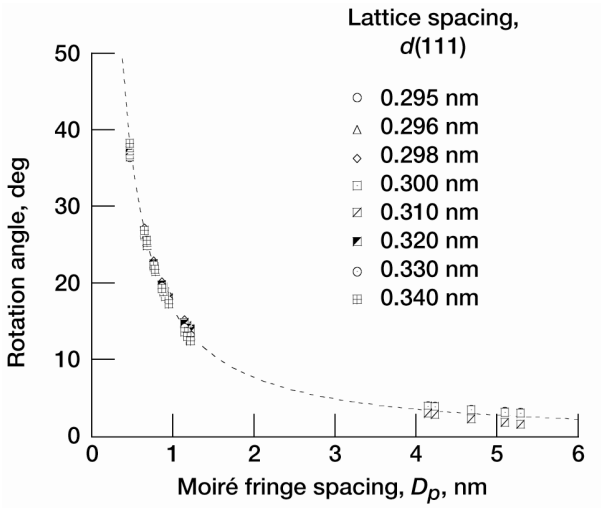

Figure 9.—Rotation angle as function of moiré pattern spacing in Nd-Yb and Gd-Yb co-doped ZrO_2-Y_2O_3-based coatings. Smaller moiré fringe spacing corresponds to defective lattice region with large relative rotation lattices, while larger moiré fringe spacing corresponds to defect region with small relative rotation lattices.

The relationship between the mixed moiré fringe pattern D_m and two contrasting lattice spacings d_1 and d_2 can be expressed by (ref. 4)

$$D_m \approx \frac{d_1 d_2}{\sqrt{(d_1 - d_2)^2 + d_1 d_2 \alpha^2}} \tag{2}$$

where α is the relative rotation angle in radiance between the two lattices. The lattice rotation angle as a function of mixed moiré fringe spacing from the (111) planes for various assumed cluster region d spacing was plotted in figure 9. It can be seen that the observed moiré fringe spacing deceases with increasing the relative lattice rotation angle between the cluster and matrix. The relative rotation angle of the cluster and matrix lattices can be determined more or less unambiguously from the observed mixed rotational moiré fringe spacing D_m of the (111) planes because the lattice spacing values are still very close in the cluster and matrix regions. For the coatings investigated in this study, the rotation angle was found to be mostly between 10 and 25°. It is also noticed that the large moiré fringe spacing (5.0 nm or higher) in some regions corresponds to the clusters with low rotation angles as is similar to the case of parallel moiré fringes.

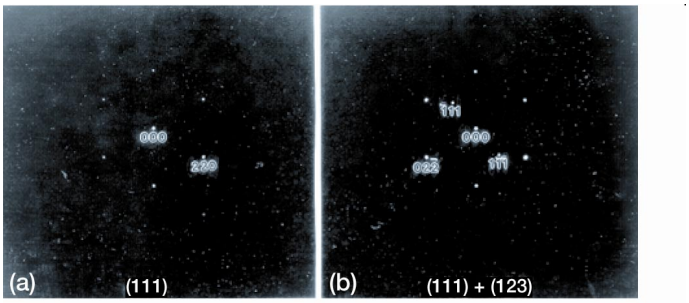

Figure 10.—Selected area electron diffraction (SAD) patterns of plasma-sprayed Nd-Yb co-doped ZrO_2-Y_2O_3 coating. (a) Matrix region. (b) Highly defective cluster region.

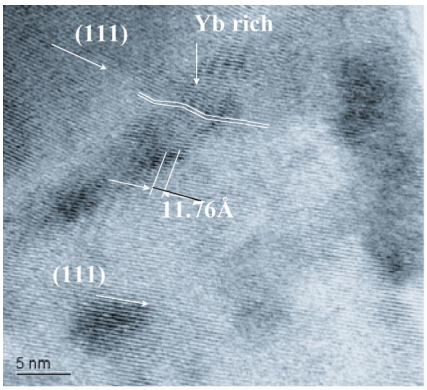

Figure 11.—Ytterbia-rich region with distorted (111) lattice planes in plasma-sprayed ZrO_2-13.5 mol% $(Y, Nd, Yb)_2O_3$ coating.

Figure 10 shows the SAD patterns in both a matrix region and a highly defective cluster region of the plasma-sprayed ZrO_2-13.5 mol% $(Y, Nd, Yb)_2O_3$ coating. The matrix region has a relatively simple diffraction pattern in the zone axis (111) orientation. However, the overlapping cluster-matrix lattice region generates a more complex diffraction pattern with the zone axis in the (111) orientation and slightly off the (111) orientation, at approximately the (123) orientation. An EDS-identified ytterbia-rich region with the distorted lattice planes of the coating is also shown in figure 11. The Sc_2O_3-added, five-component ZrO_2-based thermal barrier coatings were found to be more defective, with many small patches of the cluster regions (5 to 10 nm in size) and large rotation angles (greater than 20°) observed in the coating lattices under the TEM investigations.

The dopant-induced defect clusters are further demonstrated by the TEM high-resolution EELS analysis. Figure 12 shows the EELS compositional maps of the plasma-sprayed and EB–PVD coatings, which confirmed the significant segregations of the rare earth cluster dopants, Nd, Gd, and Yb. The

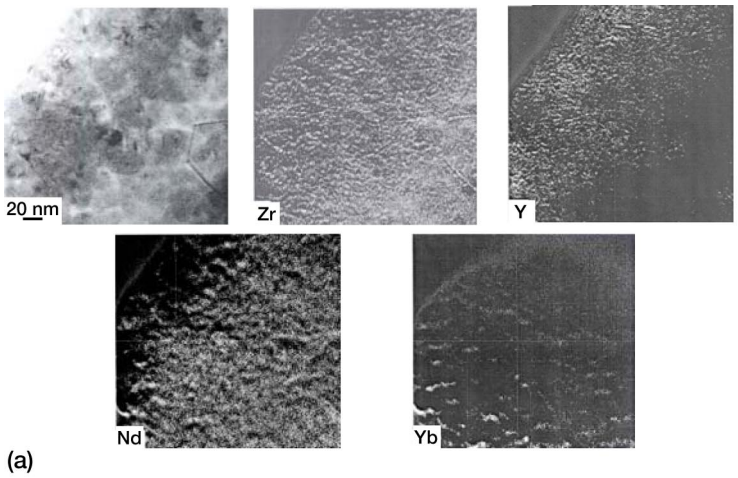

Figure 12.—EELS compositional maps of plasma-sprayed and EB–PVD defect cluster thermal barrier coatings showing significant segregations of rare earth cluster dopants, Nd, Gd, and Yb. (a) Plasma-sprayed ZrO_2-13.5 mol% $(Y, Nd, Yb)_2O_3$ coating. (b) EB–PVD ZrO_2-14 mol% $(Y, Gd, Yb)_2O_3$ coating.

segregation size ranges approximately from 20 to 100 nm. Yttrium showed relatively uniform distribution and had much less segregation as compared with the rare earth cluster dopants, despite yttrium having the highest composition among all the dopants in the coating systems. The complimentary cluster dopant segregation (i.e., the Nd (or Gd) and Yb (and/or Sc) segregated independently) is also observed from the EELS results. The complimentary cluster dopant segregation phenomenon may provide profound insight into the observed significantly lower thermal conductivity and better thermal stability of the multicomponent thermal barrier coatings as compared to the pseudobinary and even ternary coating systems.

Concluding Remarks

The addition of multicomponent rare earth dopants to zirconia-yttria-based thermal barrier coatings has been shown to significantly reduce the coating thermal conductivity and improve sintering resistance. In this study, defect clusters, induced by the addition of the dopants to the multicomponent zirconia-yttria

thermal barrier structure, were characterized using transmission electron microscopy (TEM). The parallel and mixed rotation defective lattices and defect clusters have been identified using moiré fringe patterns from the high-resolution lattice images. The extensive nanoscale cluster dopant Nd, Gd, and Yb segregation has been shown by the high-resolution electron energy-loss spectroscopy (EELS) concentration maps analysis. The cluster dopant segregation resulted in significant local lattice distortion, with the estimated lattice constant increase (with respect to the matrix lattice) greater than 5 percent in some cluster regions. The rotation angle between the cluster and matrix lattices has been found to be in the range of 0 to 35°. The presence of the 5- to 100-nm-sized defect clusters and nanophases, facilitated by the dopant composition heterogeneity and complimentary individual cluster dopant segregation, are believed to be responsible for the significant reduction of thermal conductivity, improved sintering resistance, and long-term high-temperature stability of the advanced multicomponent thermal barrier coating systems.

References

1. Zhu, Dongming; and Miller, Robert A.: Low Conductivity and Sintering-Resistant Thermal Barrier Coatings. U.S. Provisional Patent Application Serial No. 60/263,257, 2001; U.S. Patent Application Serial No. 09/904,084, 2001.
2. Zhu, Dongming; and Miller, Robert A.: Thermal Conductivity and Sintering Behavior of Advanced Thermal Barrier Coatings. Ceram. Eng. Sci. Proc., vol. 23, no. 4, 2002, pp. 457−468.
3. Zhu, Dongming, et al.: Furnace Cyclic Behavior of Plasma-Sprayed Ziconia-Yttria and Multi-Component Rare Earth Oxide Doped Thermal Barrier Coatings. Ceram. Eng. Sci. Proc., vol. 23, no. 4, 2002, pp. 533−545.
4. Hirsch, Peter Bernhard: Electron Microscopy of Thin Crystals. Butterworths, Washington, 1965.

REPORT DOCUMENTATION PAGE

Form Approved
OMB No. 0704-0188

1. AGENCY USE ONLY (*Leave blank*)	2. REPORT DATE	3. REPORT TYPE AND DATES COVERED
	January 2004	Technical Memorandum

4. TITLE AND SUBTITLE

Defect Clustering and Nanophase Structure Characterization of Multicomponent Rare Earth-Oxide-Doped Zirconia-Yttria Thermal Barrier Coatings

5. FUNDING NUMBERS

WBS–22–714–30–09
1L161102AF20

6. AUTHOR(S)

Dongming Zhu, Yuan L. Chen, and Robert A. Miller

7. PERFORMING ORGANIZATION NAME(S) AND ADDRESS(ES)

National Aeronautics and Space Administration
John H. Glenn Research Center at Lewis Field
Cleveland, Ohio 44135–3191

8. PERFORMING ORGANIZATION REPORT NUMBER

E–14018

9. SPONSORING/MONITORING AGENCY NAME(S) AND ADDRESS(ES)

National Aeronautics and Space Administration
Washington, DC 20546–0001
and
U.S. Army Research Laboratory
Adelphi, Maryland 20783–1145

10. SPONSORING/MONITORING AGENCY REPORT NUMBER

NASA TM—2004-212480
ARL–TR–3014

11. SUPPLEMENTARY NOTES

Dongming Zhu, U.S. Army Research Laboratory, NASA Glenn Research Center; Yuan L. Chen, QSS Group, Inc., Cleveland, Ohio 44135; and Robert A. Miller, NASA Glenn Research Center. Responsible person, Dongming Zhu, organization code 5160, 216–433–5422.

12a. DISTRIBUTION/AVAILABILITY STATEMENT

Unclassified - Unlimited
Subject Categories: 23, 27, and 24 Distribution: Nonstandard

Available electronically at http://gltrs.grc.nasa.gov

This publication is available from the NASA Center for AeroSpace Information, 301–621–0390.

12b. DISTRIBUTION CODE

13. ABSTRACT ***(Maximum 200 words)***

Advanced thermal barrier coatings (TBCs) have been developed by incorporating multicomponent rare earth oxide dopants into zirconia-based thermal barrier coatings to promote the creation of the thermodynamically stable, immobile oxide defect clusters and/or nanophases within the coating systems. In this paper, the defect clusters, induced by Nd, Gd, and Yb rare earth dopants in the zirconia-yttria thermal barrier coatings, were characterized by high-resolution transmission electron microscopy (TEM). The TEM lattice imaging, selected area diffraction (SAD), and electron energy-loss spectroscopy (EELS) analyses demonstrated that the extensive nanoscale rare earth dopant segregation exists in the plasma-sprayed and electron-physical-vapor-deposited (EB–PVD) thermal barrier coatings. The nanoscale concentration heterogeneity and the resulting large lattice distortion promoted the formation of parallel and rotational defective lattice clusters in the coating systems. The presence of the 5- to 100-nm-sized defect clusters and nanophases is believed to be responsible for the significant reduction of thermal conductivity, improved sintering resistance, and long-term high-temperature stability of the advanced thermal barrier coating systems.

14. SUBJECT TERMS

Thermal barrier coatings; Thermal conductivity; Defect clustering; Dopant segregation; Lattice imaging; Moiré pattern

15. NUMBER OF PAGES

17

16. PRICE CODE

17. SECURITY CLASSIFICATION OF REPORT	18. SECURITY CLASSIFICATION OF THIS PAGE	19. SECURITY CLASSIFICATION OF ABSTRACT	20. LIMITATION OF ABSTRACT
Unclassified	Unclassified	Unclassified	